# Charge asymmetry of same-sign dileptons in $B^0 - \bar{B}^0$ mixing

E. Nakano,[28] K. Abe,[7] K. Abe,[39] H. Aihara,[41] Y. Asano,[45] T. Aushev,[11] A. M. Bakich,[36] Y. Ban,[31] E. Barberio,[19] U. Bitenc,[12] I. Bizjak,[12] S. Blyth,[24] A. Bondar,[1] A. Bozek,[25] M. Bračko,[7,12,18] T. E. Browder,[6] A. Chen,[22] W. T. Chen,[22] B. G. Cheon,[3] Y. Choi,[35] A. Chuvikov,[32] J. Dalseno,[19] M. Danilov,[11] M. Dash,[46] J. Dragic,[7] A. Drutskoy,[4] S. Eidelman,[1] Y. Enari,[20] S. Fratina,[12] T. Gershon,[7] G. Gokhroo,[37] B. Golob,[12,17] T. Hara,[29] N. C. Hastings,[41] K. Hayasaka,[20] H. Hayashii,[21] M. Hazumi,[7] L. Hinz,[16] T. Hokuue,[20] Y. Hoshi,[39] S. Hou,[22] W.-S. Hou,[24] T. Iijima,[20] A. Imoto,[21] K. Inami,[20] A. Ishikawa,[7] R. Itoh,[7] M. Iwasaki,[41] J. H. Kang,[47] J. S. Kang,[14] N. Katayama,[7] H. Kawai,[2] T. Kawasaki,[27] H. R. Khan,[42] H. Kichimi,[7] H. O. Kim,[35] S. K. Kim,[34] S. M. Kim,[35] S. Korpar,[12,18] P. Križan,[12,17] P. Krokovny,[1] S. Kumar,[30] C. C. Kuo,[22] Y.-J. Kwon,[47] J. S. Lange,[5] G. Leder,[10] T. Lesiak,[25] J. Li,[33] S.-W. Lin,[24] D. Liventsev,[11] G. Majumder,[37] D. Marlow,[32] T. Matsumoto,[43] A. Matyja,[25] W. Mitaroff,[10] K. Miyabayashi,[21] H. Miyake,[29] H. Miyata,[27] R. Mizuk,[11] D. Mohapatra,[46] T. Mori,[42] T. Nagamine,[40] Y. Nagasaka,[8] M. Nakao,[7] H. Nakazawa,[7] Z. Natkaniec,[25] S. Nishida,[7] O. Nitoh,[44] S. Ogawa,[38] T. Ohshima,[20] T. Okabe,[20] S. Okuno,[13] S. L. Olsen,[6] H. Ozaki,[7] H. Palka,[25] H. Park,[15] N. Parslow,[36] R. Pestotnik,[12] L. E. Piilonen,[46] H. Sagawa,[7] Y. Sakai,[7] N. Sato,[20] T. Schietinger,[16] O. Schneider,[16] M. E. Sevior,[19] H. Shibuya,[38] V. Sidorov,[1] A. Somov,[4] R. Stamen,[7] S. Stanič,[45,*] M. Starič,[12] K. Sumisawa,[29] S. Y. Suzuki,[7] O. Tajima,[7] F. Takasaki,[7] K. Tamai,[7] N. Tamura,[27] M. Tanaka,[7] Y. Teramoto,[28] X. C. Tian,[31] K. Trabelsi,[6] T. Tsuboyama,[7] T. Tsukamoto,[7] S. Uehara,[7] T. Uglov,[11] S. Uno,[7] P. Urquijo,[19] K. E. Varvell,[36] C. C. Wang,[24] C. H. Wang,[23] M. Watanabe,[27] Q. L. Xie,[9] B. D. Yabsley,[46] A. Yamaguchi,[40] Y. Yamashita,[26] M. Yamauchi,[7] J. Ying,[31] J. Zhang,[7] L. M. Zhang,[33] Z. P. Zhang,[33] V. Zhilich,[1] and D. Žontar[12,17]

(Belle Collaboration)

[1]*Budker Institute of Nuclear Physics, Novosibirsk*
[2]*Chiba University, Chiba*
[3]*Chonnam National University, Kwangju*
[4]*University of Cincinnati, Cincinnati, Ohio 45221*
[5]*University of Frankfurt, Frankfurt*
[6]*University of Hawaii, Honolulu, Hawaii 96822*
[7]*High Energy Accelerator Research Organization (KEK), Tsukuba*
[8]*Hiroshima Institute of Technology, Hiroshima*
[9]*Institute of High Energy Physics, Chinese Academy of Sciences, Beijing*
[10]*Institute of High Energy Physics, Vienna*
[11]*Institute for Theoretical and Experimental Physics, Moscow*
[12]*J. Stefan Institute, Ljubljana*
[13]*Kanagawa University, Yokohama*
[14]*Korea University, Seoul*
[15]*Kyungpook National University, Taegu*
[16]*Swiss Federal Institute of Technology of Lausanne, EPFL, Lausanne*
[17]*University of Ljubljana, Ljubljana*
[18]*University of Maribor, Maribor*
[19]*University of Melbourne, Victoria*
[20]*Nagoya University, Nagoya*
[21]*Nara Women's University, Nara*
[22]*National Central University, Chung-li*
[23]*National United University, Miao Li*
[24]*Department of Physics, National Taiwan University, Taipei*
[25]*H. Niewodniczanski Institute of Nuclear Physics, Krakow*
[26]*Nihon Dental College, Niigata*
[27]*Niigata University, Niigata*
[28]*Osaka City University, Osaka*
[29]*Osaka University, Osaka*
[30]*Panjab University, Chandigarh*
[31]*Peking University, Beijing*
[32]*Princeton University, Princeton, New Jersey 08544*
[33]*University of Science and Technology of China, Hefei*
[34]*Seoul National University, Seoul*
[35]*Sungkyunkwan University, Suwon*

[36]*University of Sydney, Sydney NSW*
[37]*Tata Institute of Fundamental Research, Bombay*
[38]*Toho University, Funabashi*
[39]*Tohoku Gakuin University, Tagajo*
[40]*Tohoku University, Sendai*
[41]*Department of Physics, University of Tokyo, Tokyo*
[42]*Tokyo Institute of Technology, Tokyo*
[43]*Tokyo Metropolitan University, Tokyo*
[44]*Tokyo University of Agriculture and Technology, Tokyo*
[45]*University of Tsukuba, Tsukuba*
[46]*Virginia Polytechnic Institute and State University, Blacksburg, Virginia 24061*
[47]*Yonsei University, Seoul*

We report a measurement of the charge asymmetry for same-sign dileptons in $B^0 - \bar{B}^0$ mixing, $A_{sl}$. The data were collected with the Belle detector at KEKB. Using a data sample of 78 fb$^{-1}$ recorded at the $\Upsilon(4S)$ resonance and 9 fb$^{-1}$ recorded at an energy 60 MeV below the resonance, we measure $A_{sl} = (-1.1 \pm 7.9(\text{stat}) \pm 8.5(\text{sys})) \times 10^{-3}$.

## I. INTRODUCTION

The standard model allows $CP$ violation in $B^0 - \bar{B}^0$ mixing [1]. In particular, there is a possible difference between the $B^0 \rightarrow \bar{B}^0$ and $\bar{B}^0 \rightarrow B^0$ transition rates that can manifest itself as a charge asymmetry in same-sign dilepton events in $\Upsilon(4S)$ decays when prompt leptons from semileptonic decays of neutral $B$ mesons are selected. With the assumption of $CPT$ invariance, the flavor and mass eigenstates of the neutral $B$ mesons are related by

$$|B_H\rangle = p|B^0\rangle + q|\bar{B}^0\rangle, \qquad |B_L\rangle = p|B^0\rangle - q|\bar{B}^0\rangle, \quad (1)$$

where $|p|^2 + |q|^2 = 1$. The time-dependent decay rate for same-sign dileptons is given by

$$\Gamma_{\Upsilon(4S)\rightarrow\ell^+\ell^+}(\Delta t) = \frac{|A_\ell|^4}{8\tau_{B^0}} e^{-|\Delta t|/\tau_{B^0}} \left|\frac{p}{q}\right|^2$$
$$\times \left[\cosh\left(\frac{\Delta\Gamma}{2}\Delta t\right) - \cos(\Delta m_d \Delta t)\right] \quad (2)$$

for the $\ell^+\ell^+$ sample. For the $\ell^-\ell^-$ sample, $p/q$ is replaced by $q/p$. Here $\Delta m_d$ and $\Delta\Gamma$ are the differences in mass and decay width between the two mass eigenstates, $\tau_{B^0}$ is the average lifetime of the two mass eigenstates, and $\Delta t$ is the proper time difference between the two $B$ meson decays. In this analysis only the absolute value of $\Delta t$ is used. It is assumed that the semileptonic decay of the neutral $B$ meson is flavor specific and $CP$ conserving, so that $A_\ell = \bar{A}_\ell$, where $A_\ell \equiv \langle X^- \ell^+ \nu_\ell | B^0 \rangle$ and $\bar{A}_\ell \equiv \langle X^+ \ell^- \bar{\nu}_\ell | \bar{B}^0 \rangle$. If $CP$ is not conserved in mixing, the condition $|p/q| = 1$ is no longer true and the decay rates for $\ell^+\ell^+$ and $\ell^-\ell^-$ samples can differ. As can be seen in Eq. (2), the $\Delta t$ dependence is the same for the $\ell^+\ell^+$ and $\ell^-\ell^-$ samples, and therefore the $CP$ violation shows up as a $\Delta t$-independent charge asymmetry, defined as

---

*On leave from Nova Gorica Polytechnic, Nova Gorica

$$A_{sl} \equiv \frac{\Gamma_{\Upsilon(4S)\rightarrow\ell^+\ell^+} - \Gamma_{\Upsilon(4S)\rightarrow\ell^-\ell^-}}{\Gamma_{\Upsilon(4S)\rightarrow\ell^+\ell^+} + \Gamma_{\Upsilon(4S)\rightarrow\ell^-\ell^-}} = \frac{1 - |q/p|^4}{1 + |q/p|^4}$$
$$\simeq \frac{4\,\text{Re}(\epsilon_B)}{1 + |\epsilon_B|^2}. \quad (3)$$

Here $\epsilon_B$ corresponds to the $\epsilon_K$ describing $CP$ violation in the neutral $K$ meson system. Standard model calculations give the size of this asymmetry to be at or below the order of $10^{-3}$ [2–4]. A significantly larger value would therefore be an indication of new physics [5].

Experimentally, a measurement of same-sign dilepton events that originate from $B^0 B^0$ and $\bar{B}^0 \bar{B}^0$ initial states requires careful charge-dependent corrections, which are done in several steps. First, the contribution from continuum $e^+ e^- \rightarrow q\bar{q}$ (where $q = u$, $d$, $s$ or $c$) to same-sign dilepton events is subtracted using off-resonance data. Second, all detected lepton tracks are corrected for charge asymmetries in the efficiencies for track finding and lepton identification, and for the probabilities of misidentifying hadrons as leptons. After these corrections, the remaining same-sign dilepton events still contain backgrounds from $B^0 \bar{B}^0$ and $B^+ B^-$ events. The last step of this analysis is to separate the signal events from these background events using their different behavior in the $\Delta t$ distributions.

## II. BELLE DETECTOR

This analysis is based on a data sample of 78 fb$^{-1}$ at the $\Upsilon(4S)$ resonance ("on-resonance") and 9 fb$^{-1}$ at 60 MeV below the $\Upsilon(4S)$ resonance ("off-resonance") collected with the Belle detector [6] at the KEKB asymmetric $e^+ e^-$ collider [7]. The Belle detector is a large-solid-angle magnetic spectrometer that consists of a three-layer silicon vertex detector (SVD), a 50-layer central drift chamber (CDC) for tracking, a mosaic of aerogel threshold Cherenkov counters (ACC), time-of-flight scintillation

counters (TOF), and an array of CsI(Tl) crystals for electromagnetic calorimetry (ECL) located inside of a superconducting solenoid coil that provides a 1.5 T magnetic field. An iron flux-return located outside of the coil is instrumented to detect $K_L^0$ mesons and to identify muons (KLM).

## A. Track finding efficiency

We have tried two different methods to obtain track finding efficiecny. First, we use a clean sample of $D^0 \rightarrow K_S^0 \pi^+ \pi^-$ followed by $K_S^0 \rightarrow \pi^+ \pi^-$ in the $D^{*+} \rightarrow D^0 \pi^+$ decay chain. Since this process has over-constraining information, the signal yield can be obtained either by requiring the presence of both pions from the $K_S^0$ decays or by requiring only one of them, and therefore a difference of the two yields gives the absolute measurements of the track finding efficiency for $\pi^+$ and $\pi^-$ separately. This study shows that the data and Monte Carlo (MC) simulations are in good agreement within 1% accuracy for the efficiency and there is no charge asymmetry. Although this is a clean measurement, it has limited statistical accuracy and limited laboratory momentum range.

The track finding efficiency that is used in further analyses is determined by analyzing a sample where simulated single electron or muon tracks are overlaid on hadronic events taken from experimental data. Lepton tracks are generated to cover the region of $1.2 \text{ GeV}/c < p^* < 2.3 \text{ GeV}/c$ and $30° < \theta_{\text{lab}} < 135°$, where $p^*$ is the lepton momentum in the $e^+e^-$ center-of-mass (c.m.) frame. The $z$ axis passes through the nominal interaction point, and is antiparallel to the positron beam direction. The track find-

ing efficiencies are obtained for each bin of $p^*$ (1.2–1.3, 1.3–1.4, 1.4–1.5, 1.5–1.6, 1.6–1.8, 1.8–2.0 and 2.0–2.3 GeV/$c$), and $\theta_{\text{lab}}$ (30°–37°, 37°–50°, 50°–77°, 77°–82°, 82°–111°, 111°–119°, 119°–128° and 128°–135°). Figure 1 shows $\theta_{\text{lab}}$-averaged track finding efficiencies for positive and negative tracks separately and their fractional differences as functions of $p^*$ for electron and muon tracks. Events in all $\theta_{\text{lab}}$ regions are combined in these plots. The charge dependence of the track finding efficiency for both electrons and muons is less than 0.5%.

## B. Lepton identification

The most important contribution to the electron identification comes from examination of the ratio of the ECL cluster energy to the track momentum measured in the CDC. This information is combined with the shower measurement in the ECL, the specific ionization measurements $(dE/dx)$ in the CDC, matching information between the ECL cluster position and extrapolated position of the CDC track, and the ACC light yield to form an electron likelihood $\mathcal{L}_e$ [8].

The two-photon process $e^+e^- \rightarrow (e^+e^-)e^+e^-$, where the beam particles $(e^+e^-)$ escape detection and only $e^+e^-$ are detected, is used to estimate the electron identification efficiency. For this data sample, events are required to have: (i) two tracks with particle identification information inconsistent with a muon hypothesis, laboratory momenta greater than 0.5 GeV/$c$ and transverse momenta greater than 0.25 GeV/$c$; (ii) at least one ECL cluster with energy greater than 20 MeV. The two tracks are required to have: (i) an acolinearity angle whose cosine is greater than
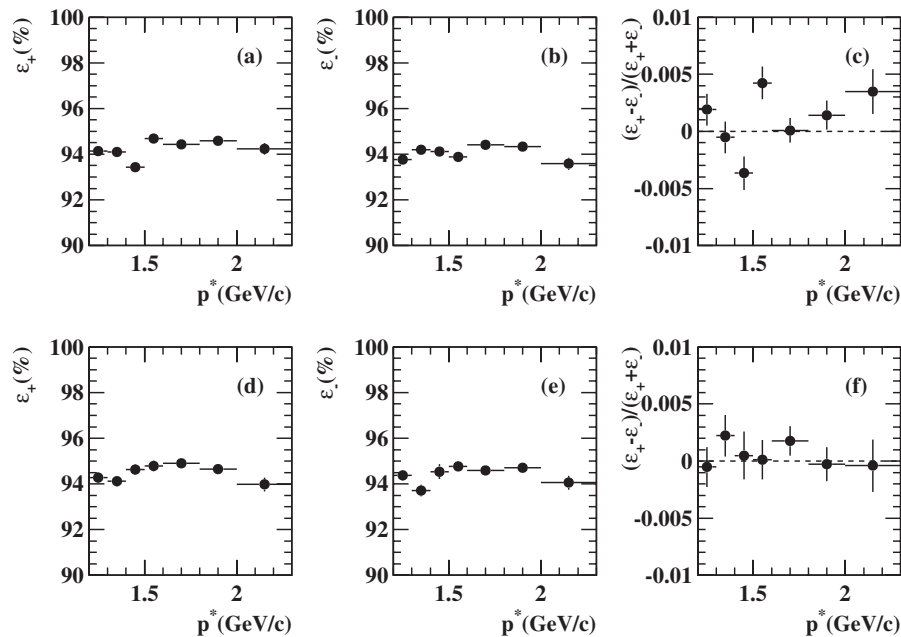


FIG. 1. $\theta_{\text{lab}}$-averaged track finding efficiencies as a function of c.m. momentum for positron tracks $\varepsilon_+$ (a), electron tracks $\varepsilon_-$ (b), and charge dependence defined as $(\varepsilon_+ - \varepsilon_-)/(\varepsilon_+ + \varepsilon_-)$ (c). Corresponding plots for muon tracks are shown in (d), (e), and (f).

$-0.997$; (ii) a transverse-momentum sum less than 0.2 GeV/$c$; (iii) a longitudinal momentum sum of less than 2.5 GeV/$c$ in the c.m. frame; (iv) an invariant mass less than 5 GeV/$c^2$. In addition, the sum of the ECL cluster energies has to be between 0.6 GeV and 6.0 GeV. A MC simulation study shows that these requirements select the $e^+e^- \rightarrow (e^+e^-)e^+e^-$ events with 99.5% purity. The electron identification efficiency is obtained by taking the ratio of the number of tracks selected among this sample with and without additional electron identification requirements.

For muon identification, CDC tracks are extrapolated to the KLM and the measured range and transverse deviation in the KLM is compared with the expected values to form a muon likelihood $\mathcal{L}_\mu$ [9]. We determine the muon identification efficiency by analyzing a data sample where a simulated muon track is overlaid on a hadronic event taken from the experimental data rather than using the two-photon $\mu^+\mu^-$ events. This is because, while the two-photon events provide a good data sample for evaluating the charge-dependent bias, it is not suitable for the purpose of evaluating the absolute value of the efficiency due to a contamination from two-photon $\tau^+\tau^-$ events. A charge-dependent bias that we observe in the two-photon $\mu^+\mu^-$ data [9] is in agreement with that determined from the method we apply here.

The lepton identification efficiencies are obtained in the same $p^*$ and $\theta_{\text{lab}}$ bins used for the track finding efficiency study. Figure 2 shows the $\theta_{\text{lab}}$-averaged charge-dependent lepton identification efficiencies, where electron tracks are required to satisfy $\mathcal{L}_e > 0.8$, and the muon tracks are required to satisfy $\mathcal{L}_\mu > 0.9$ and to have a reduced $\chi^2$

value for their transverse deviations in the KLM of less than 3.5. The charge dependence of the identification efficiency is less than 0.5% for both electrons and muons. Exactly the same criteria are imposed to select signal leptons.

### C. Hadron misidentification

The hadron fake rate, which is defined as the probability that a hadron track is misidentified as a lepton, is determined from a sample of $K_S^0 \rightarrow \pi^+\pi^-$ decays for pions, $\phi \rightarrow K^+K^-$ decays for kaons, and $\Lambda \rightarrow p\pi^-$ ($\bar{\Lambda} \rightarrow \bar{p}\pi^+$) decays for protons. These decays are selected from a hadronic event sample described below. To select these track-pair combinations, the distance of closest approach with respect to the run-dependent interaction point and the position of the decay vertex are used. The difference in $z$ position of the two tracks and the angle between position vector of the decay vertex and the momentum vector of $K_S^0$ or $\Lambda(\bar{\Lambda})$ in $r$-$\phi$ plane at the decay vertex are also used. To evaluate the fake rate for positive charged pions, the yield of $K_S^0$ mesons reconstructed before and after applying lepton identification to the $\pi^+$ are compared. The momentum dependence of the fake rate is evaluated by performing the analysis in bins of $\pi^+$ laboratory frame momentum. The $K_S^0$ yields are obtained by fitting the invariant mass distributions to the sum of a double Gaussian signal and a smooth background function. The fake rate for negative pions is obtained by repeating this procedure with the roles of the positive and negative tracks reversed. The same procedure is employed to for $\psi$ and $\Lambda(\bar{\Lambda})$ to obtain the fake rates of $K^\pm$ and $p(\bar{p})$.
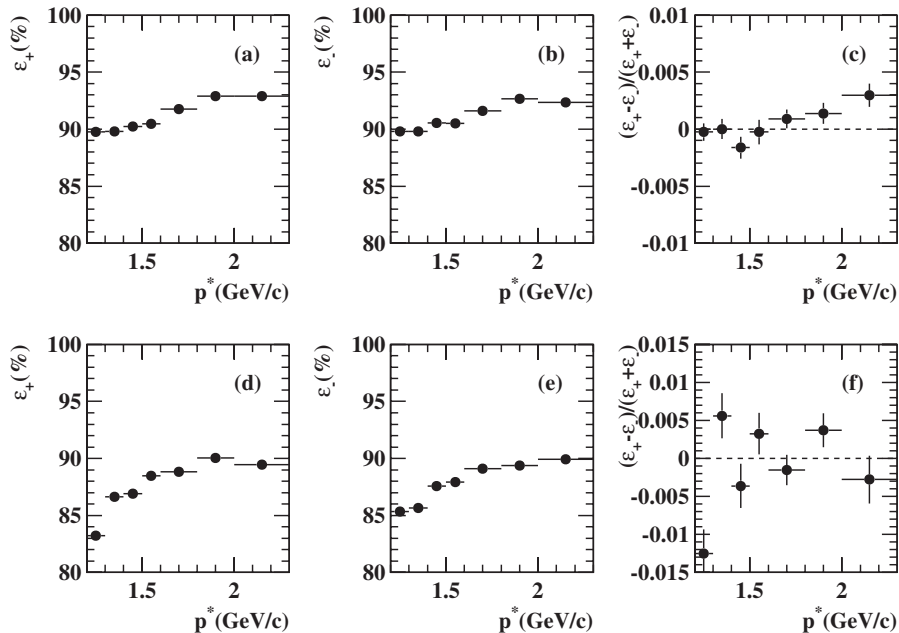


FIG. 2. $\theta_{\text{lab}}$-averaged identification efficiencies as a function of c.m. momentum for positrons $\varepsilon_+$ (a), electrons $\varepsilon_-$ (b), and charge dependence defined as $(\varepsilon_+ - \varepsilon_-)/(\varepsilon_+ + \varepsilon_-)$ (c). Corresponding plots for muons are shown in (d), (e), and (f).
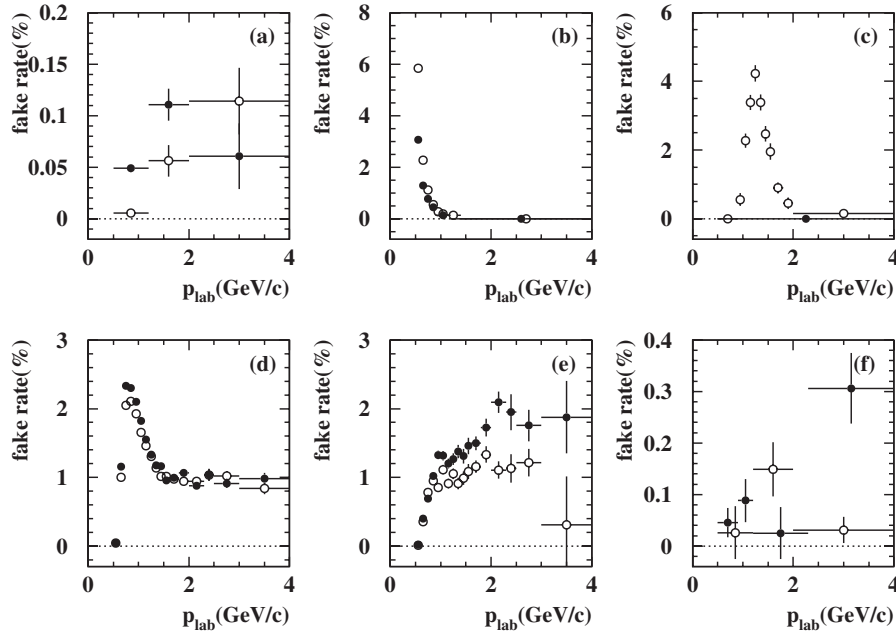
FIG. 3.   Rates of hadrons faking leptons vs laboratory momentum: (a) $\pi \to e$, (b) $K \to e$, (c) $p \to e$, (d) $\pi \to \mu$, (e) $K \to \mu$, (f) $p \to \mu$. Filled circles are for positive tracks and open circles are for negative tracks. The increase in the rate of kaons faking electrons at low momentum clearly visible in (b) is due to the overlap of the electron and kaon energy-loss bands; the other distributions are discussed in the text. Note that the minimum values of vertical axes are set to negative values. The dotted lines shows fake rate equal to zero.

In this study, because of low statistics, $\theta_{\text{lab}}$-averaged values are used, and some momentum bins are combined.

Figure 3 shows the hadron fake rates as a function of momentum in the laboratory frame. The rate of pions faking electrons is at most 0.1% for both charges. The rate of kaons faking electrons decreases rapidly as $p_{\text{lab}}$ becomes larger and is less than 0.2% for $p_{\text{lab}} > 1.4$ GeV/$c$, with no significant charge dependence. While the rate of protons faking positrons is nearly zero, the rate for antiprotons faking electrons is as large as 4% due to the large antiproton annihilation cross section in the ECL. Because of low statistics, the rate of protons faking positrons is obtained from the $\theta_{\text{lab}}$-averaged value over all momenta. The rate of pions faking muons is about 1% for $p_{\text{lab}} > 1.5$ GeV/$c$ and shows no significant charge dependence. The rate of kaons faking muons is 1% to 2%, with that for $K^+$ being about 50% larger than that for $K^-$ due to the larger kaon-nucleon cross section for the $K^-$. The rate of protons faking muons is less than 0.4% and shows no clear charge dependence.

## III. EVENT SELECTION

### A. Hadronic event selection

Hadronic events are required to have at least five tracks, an event vertex with radial and $z$ coordinates within 1.5 cm and 3.5 cm, respectively, of the nominal beam interaction point, a total reconstructed c.m. energy greater than 0.5 W (W is the c.m. energy), a net reconstructed c.m. momentum with a $z$ component less than 0.3 W/$c$, a total energy deposited in the ECL between 0.025 and 0.9 W, and a ratio $R_2$ of the second and zeroth Fox-Wolfram moments [10] of less than 0.7.

### B. Dilepton event selection

Lepton candidates are selected from among the charged tracks by requiring the criteria previously described. In both electron and muon cases, a distance of closest approach to the run-dependent interaction point less than 0.05 cm radially and 2.0 cm in $z$ is required. At least one SVD hit per track in the $r$-$\phi$ view and two SVD hits in the $r$-$z$ view are required. To eliminate electrons from $\gamma \to e^+ e^-$ conversions, electron candidates are paired with all other oppositely charged tracks and the invariant mass (assuming the electron mass) $M_{e^+ e^-}$ is calculated. If $M_{e^+ e^-} < 100$ MeV/$c^2$, the electron candidate is rejected. If a hadronic event contains more than two lepton candidates, the two with the highest c.m. momenta are used.

The two lepton candidates must satisfy additional criteria. The c.m. momentum of each lepton is required to be in the range 1.2 GeV/$c < p^* < 2.3$ GeV/$c$. The lower threshold reduces contributions from secondary charm decay; the upper threshold reduces continuum contributions. Each lepton track must be in the range $30° < \theta_{\text{lab}} < 135°$, where it has better $z$ vertex resolution and lepton identification. Events that contain one or more $J/\psi$ candidates are rejected. The invariant mass of each candidate lepton paired with each oppositely charged track (assum-
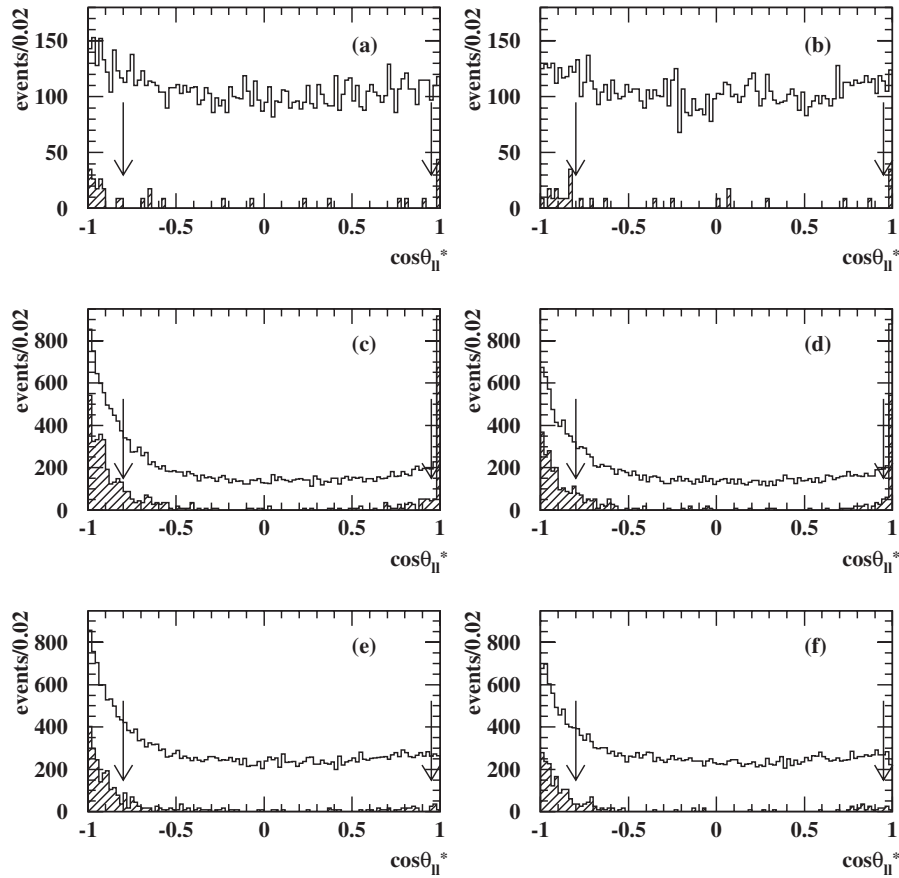
FIG. 4. $\cos\theta_{\ell\ell}^*$ distributions for dilepton samples in the on-resonance (open histogram) and scaled off-resonance (filled histogram) data. (a),(b) show $ee$ events, (c),(d) show $\mu\mu$ events and (e),(f) are from $e\mu$ combinations. (a),(c) and (e) are the $++$ charge case and (b), (d) and (f) are the $--$ charge case. The arrows indicate the selection requirements.

ing the corresponding lepton mass) is calculated. If the invariant mass falls within the $J/\psi$ region, defined as $-0.15 \text{ GeV}/c^2 < (M_{e^+e^-} - M_{J/\psi}) < 0.05 \text{ GeV}/c^2$ or $-0.05 \text{ GeV}/c^2 < (M_{\mu^+\mu^-} - M_{J/\psi}) < 0.05 \text{ GeV}/c^2$, the candidate event is rejected. The looser lower mass window for the electron pair invariant mass accommodates bremsstrahlung of the daughter electron(s).

As can be seen in Fig. 4, distributions of the opening angle of the two tracks in the c.m. frame, $\cos\theta_{\ell\ell}^*$, for the $\mu\mu$ and $e\mu$ pairs show distinct peaks in the back-to-back direction ($\cos\theta_{\ell\ell}^* \simeq -1$). This background is caused by hadron tracks misidentified as muons among jetlike con-

tinuum events. Also, spikes can be seen at $\cos\theta_{\ell\ell}^* = 1$ for the $\mu\mu$ pair events. This structure is caused by jetlike continuum events where a nonmuon track is identified as a muon because hits in the KLM from a nearby true muon are assigned to it. The dilepton opening angle in the c.m. frame $\theta_{\ell\ell}^*$ is required to satisfy $-0.80 < \cos\theta_{\ell\ell}^* < 0.95$ in order to reduce this background.

With these selection criteria there are 46 533 positive and 45 477 negative same-sign dilepton events found in the on-resonance data. Continuum contributions are estimated to be 2230 for positive and 1574 for negative same-sign events, based on the yield from off-resonance data. To

TABLE I. Summary of the dilepton yields. The yields in Continuum are determined from the yields in Off-resonance by correcting for luminosity and cross section.

| Combination | On-resonance positive | On-resonance negative | Off-resonance positive | Off-resonance negative | Continuum positive | Continuum negative |
|---|---|---|---|---|---|---|
| $ee$ | 9059 | 9028 | 11 | 11 | $96.2 \pm 28.9$ | $96.2 \pm 28.9$ |
| $\mu\mu$ | 14672 | 14014 | 144 | 100 | $1259.2 \pm 104.9$ | $874.4 \pm 87.4$ |
| $e\mu$ | 22802 | 22435 | 100 | 69 | $874.4 \pm 87.4$ | $603.4 \pm 72.6$ |
| total | 46533 | 45477 | 255 | 180 | $2229.8 \pm 139.6$ | $1574.0 \pm 117.3$ |

estimate the continuum contribution from off-resonance data, off-resonance yields were scaled by the integrated luminosities and cross section ratio. The scaling factor is defined by

$$f = \frac{\int \mathcal{L}_{\text{on}} dt}{\int \mathcal{L}_{\text{off}} dt} \frac{s_{\text{off}}}{s_{\text{on}}}, \qquad (4)$$

where $\int \mathcal{L}_{\text{on(off)}} dt$ and $s_{\text{on(off)}}$ are the integrated luminosities and the square of c.m. energies for on(off)-resonance, respectively.

These dilepton yields, decomposed into three lepton categories, are given in Table I.

### C. $\Delta z$ determination

Although the charge asymmetry of same-sign dileptons arising from $CP$ violation is independent of $\Delta t$, we use $\Delta t$ to separate the signal events from the background. The value of $\Delta t$ is related to the experimentally measurable quantity $\Delta z$ by $\Delta z \simeq \gamma \beta \Delta t$ where $\gamma \beta = 0.425$ is the Lorentz boost factor at KEKB, and $|\Delta z| = |z_1 - z_2|$ with $z_{1(2)}$ being the $z$-coordinate of the more(less) energetic lepton. The $z$-coordinate of each $B$ meson decay vertex is the production point of the daughter lepton, which is

determined from the intersection of the lepton track with the run-dependent profile of the interaction point.

### D. Subtraction of continuum events

A sample of dilepton events originating from $B\bar{B}$ events is obtained by subtracting the luminosity and cross section scaled off-resonance data from the on-resonance data. Since the kinematics of dilepton candidates in $B\bar{B}$ decays is different from those in continuum events in each of the variables $(p_1^*, p_2^*, \theta_1^*, \theta_2^*, \theta_{\ell\ell}^*, \Delta z)$, where $\theta_{1(2)}^*$ is the polar angle in the c.m. frame with respect to the beam axis of the more (less) energetic lepton, the subtraction should, in principle, be performed in this six-dimensional space, separately for each lepton flavor and charge combination.

Given the available statistics, this approach is not possible. Instead, we perform the subtraction by weighting the on-resonance and off-resonance yields for one of the six kinematical variables, while integrating over the five other variables. We obtain weighting factors for the six variables by repeating this procedure. Since, to a first approximation, the six variables are not correlated with each other, this approach provides the $B\bar{B}$ yield in the six variable space. The weighting factors are given by $w(k) = (1/r_{BB}) \times (N_{\text{on}}(k) - fN_{\text{off}}(k))/N_{\text{on}}(k)$ where $k$ denotes each of six
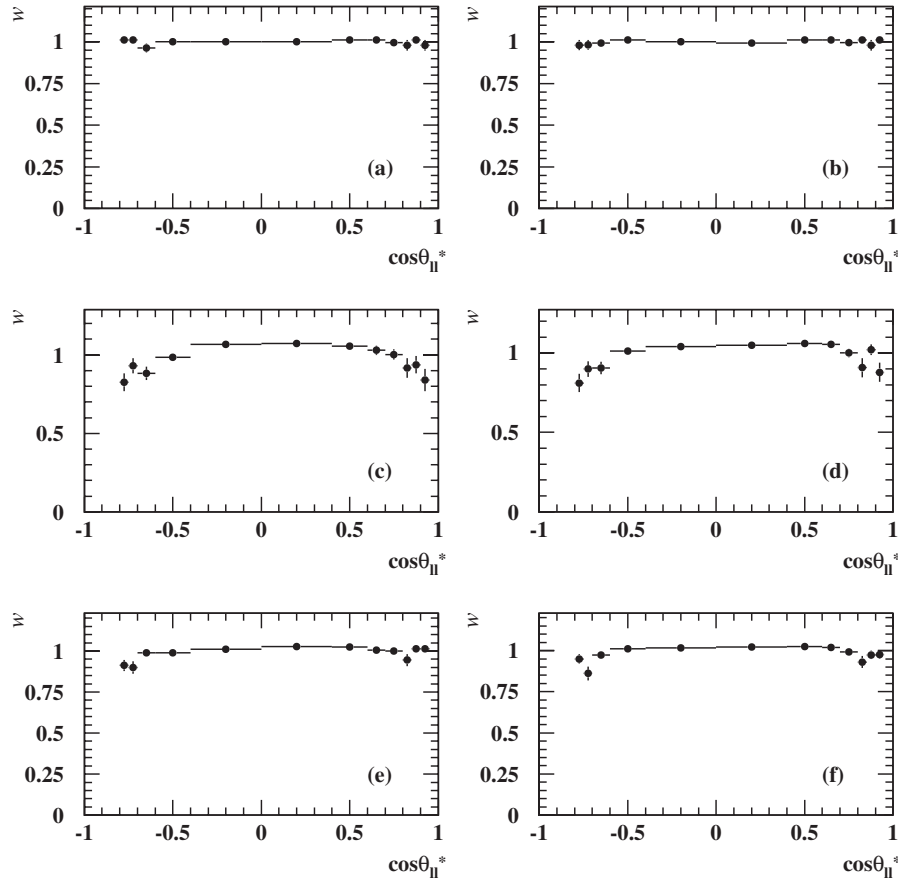


FIG. 5. $\cos\theta_{\ell\ell}^*$ dependence of the weighting factor for the fraction of the dilepton yield originating from $B\bar{B}$ decays in the on-resonance data for $e^+e^+$ (a) and $e^-e^-$ (b) and corresponding quantities for $\mu\mu$ (c) and (d) and $e\mu$ (e) and (f).

variables, $f$ is the scaling factor for the luminosity and c.m. energy introduced in Eq. (4), and $r_{BB} \equiv N_{B\bar{B}}^{\text{total}}/N_{\text{on}}^{\text{total}}$ is the fraction of total $B\bar{B}$ events in the on-resonance yield after integrating over all six variables; it is used for normalization. While the weighting factors show very little dependence on $p_1^*$, $p_2^*$, $\theta_1^*$, and $\theta_2^*$ for all combinations of lepton flavors and charges, a clear dependence is observed for $\theta_{\ell\ell}^*$ in the case of the $\mu\mu$ and $e\mu$ data samples as shown in Fig. 5. A clear dependence on $\Delta z$ is also seen for all lepton pair combinations.

Using this method, the dilepton candidate yield for each lepton flavor and charge combination is then given in terms of the on-resonance yield and the weighting factors by

$$N_{B\bar{B}}(p_1^*, p_2^*, \theta_1^*, \theta_2^*, \theta_{\ell\ell}^*, \Delta z) = r_{BB}\prod_k w(k)N_{\text{on}}(p_1^*, p_2^*, \theta_1^*,$$
$$\theta_2^*, \theta_{\ell\ell}^*, \Delta z). \qquad (5)$$

The $\Delta z$ distributions of the dilepton yields are obtained by projecting $N_{B\bar{B}}(p_1^*, p_2^*, \theta_1^*, \theta_2^*, \theta_{\ell\ell}^*, \Delta z)$ onto the $|\Delta z|$ axis.

## IV. RESULT

### A. Corrections to lepton candidates

The number of detected leptons for each lepton flavor and charge $N_{\text{det}}^{\pm}$ is related to the background-subtracted and efficiency corrected estimate of the number of leptons (true leptons) $N_{\ell}^{\pm}$ by

$$N_{\text{det}}^{\pm}(p^*, \theta_{\text{lab}}) = N_{\ell}^{\pm}(p^*, \theta_{\text{lab}})\varepsilon_{\text{trk}}^{\pm}(p^*, \theta_{\text{lab}})\bigg\{\varepsilon_{\text{pid}}^{\pm}(p^*, \theta_{\text{lab}})$$
$$+ \sum_{h=\pi,K,p} r_{h\ell}^{\pm}(p^*, \theta_{\text{lab}})\eta_{h\ell}^{\pm}(p^*, \theta_{\text{lab}})\bigg\}, \qquad (6)$$

where $\varepsilon_{\text{trk}}^{\pm}$ and $\varepsilon_{\text{pid}}^{\pm}$ are the efficiencies for track finding and lepton identification, $r_{h\ell}^{\pm}$ is the relative multiplicity of hadron of type $h$ with respect to leptons of type $\ell$ in $B\bar{B}$ event, and $\eta_{h\ell}^{\pm}$ is the rate of hadrons $h$ faking leptons $\ell$. The relative multiplicities are determined from $B\bar{B}$ MC events, and are shown in Fig. 6. The relative multiplicities include the effects of decay-in-flight and interaction with the detector.

Using the measured efficiencies, fake rates and the MC-determined relative multiplicities, the correction factors $N_{\ell}/N_{\text{det}}$ are determined in 7 bins of $p^*$ (1.2–1.3, 1.3–1.4, 1.4–1.5, 1.5–1.6, 1.6–1.8, 1.8–2.0 and 2.0–2.3 Gev/$c$), and 8 bins of $\theta_{\text{lab}}$ (30°−37°, 37°−50°, 50°−77°, 77°−82°, 82°−111°, 111°−119°, 119°−128° and 128°−135°). (The fake rates are measured in the laboratory frame, but are converted into $p^*$- and $\theta_{\text{lab}}$-dependent measurements for this correction.)

After the correction, the dilepton sample contains true leptons that come either from prompt neutral $B$ meson decay (signal) or from background processes such as charged $B$ meson decay, secondary charm decay, or other leptonic $B$ meson processes.
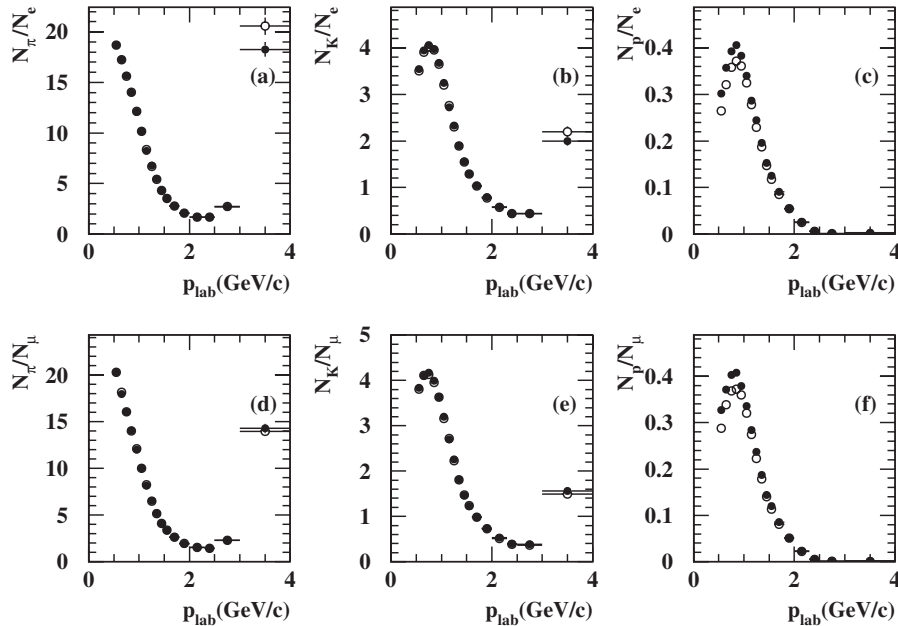


FIG. 6.    Relative multiplicities of hadrons as a function of $p_{\text{lab}}$ with respect to leptons. (a), (b) and (c) are for electrons and (d), (e) and (f) are for muons. (a) and (d) are pion to lepton, (b) and (e) are kaon to lepton, (c) and (f) are proton to lepton ratios. Filled circles are for positive tracks and open circles are for negative tracks. The effects of decay-in-flight and interaction with detector are included. Though in (a), (b), (d) and (e), the difference between positive and negative cases is less than 1%, in both (c) and (f), the proton rate is larger than the antiproton rate by about 8%. The increases in multiplicities for pions and kaons around 3.5 GeV/$c$ are due to two-body hadronic $B$ decays.

## B. Fit to $\Delta z$ distribution

A binned maximum likelihood fit with signal and background contributions is used to extract $A_{sl}(|\Delta z|)$ from the $\Delta z$ distribution. The overall background level is obtained from a fit with positive $(++)$ and negative $(--)$ samples combined.

### 1. Signal shape

In this fit the $\Delta z$ distribution for signal events is given by

$$P^{SS} \propto e^{-|\Delta t|/\tau_{B^0}}\{1 - \cos(\Delta m_d \Delta t)\}, \tag{7}$$

convolved with the detector response function described below. Equation (7) is derived from Eq. (2), assuming $\Delta \Gamma$ is small [11]. Here, $\tau_{B^0}$ and $\Delta m_d$ are fixed to their world average values [11].

In order to estimate the effect of detector resolution in the $\Delta z$ distribution, $J/\psi$ decays to $e^+e^-$ and $\mu^+\mu^-$ are used. In these events, the two tracks originate from the same point, so the measured $\Delta z$, after the background contribution is subtracted, yields the detector resolution. Candidate $J/\psi$ mesons are selected using the same require-

ments used for dilepton events, except for the $J/\psi$ veto. The $J/\psi$ signal regions are defined as $3.00$ GeV$/c^2 < M(e^+e^-) < 3.14$ GeV$/c^2$　　and　　$3.05$ GeV$/c^2 < M(\mu^+\mu^-) < 3.14$ GeV$/c^2$ and the sideband region as $3.18$ GeV$/c^2 < M(\ell^+\ell^-) < 3.50$ GeV$/c^2$ for both electrons and muons.

The invariant mass distributions of $J/\psi$ candidates are fitted to a function given by

$$N(M) = h_0 e^{-(M-M_0)^2/2S^2} + h_1 e^{-(M-M_0)^2/2\sigma_1{}^2}$$
$$+ A(M - B)^2 + C. \tag{8}$$

Here, $h_0$ and $h_1$ are the normalizations of the two Gaussians used to describe the signal, $M_0$ is the Gaussian mean which is common to both Gaussians. $\sigma_1$ is the standard deviation of the second Gaussian. A parameter $S$, defined as $S = \sigma_0$ for $M \geq M_0$ and $S = \sigma_0 + \alpha(M - M_0)$ for $M < M_0$, where $\sigma_0$ is the standard deviation of the first Gaussian, is introduced to modify the lower mass tail of the first Gaussian to take the effect of bremsstrahlung into account. $A$, $B$ and $C$ are the parameters of the background function. The $\Delta z$ distribution of the sideband re-
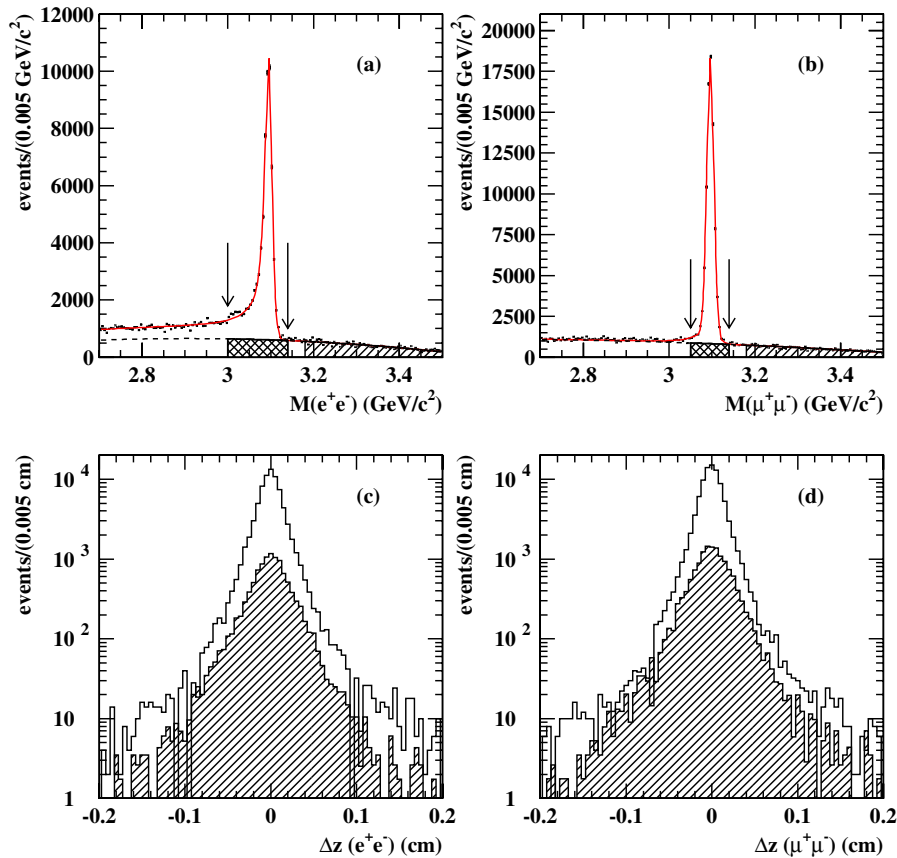


FIG. 7 (color online).　Mass distributions for $J/\psi \rightarrow e^+e^-$ (a) and $J/\psi \rightarrow \mu^+\mu^-$ (b). The arrows indicate the selection criteria for each decay mode. The dashed lines indicate the fitted background component and the solid lines show the total fit results. The cross hatched area shows the estimated combinatorial background in the signal region and the single hatched area is the sideband region used to estimate the background $\Delta z$ distribution. The $\Delta z$ distributions for $J/\psi \rightarrow e^+e^-$ (c) and $J/\psi \rightarrow \mu^+\mu^-$ (d). Open histograms are for all $J/\psi$ candidates in the signal region and hatched histograms are for the background.

gion is scaled to the background yield in the signal region and subtracted from the signal region $\Delta z$ distribution.

The $J/\psi$ mass distributions and the $\Delta z$ distributions are shown in Fig. 7. The RMS values of the $\Delta z$ distributions are 193 $\mu$m for $J/\psi \to e^+e^-$, 177 $\mu$m for $J/\psi \to \mu^+\mu^-$, and 185 $\mu$m for the combined $J/\psi \to \ell^+\ell^-$ sample.

### *2. Background shape*

The backgrounds are divided into two categories: correctly tagged (CT), and wrongly tagged (WT). The CT category mainly contains events in which both leptons come from secondary charm decay in $B^0\bar{B}^0 \to B^0 B^0 (\bar{B}^0 \bar{B}^0)$ (mixed) processes. The WT category contains events in which one lepton is from secondary charm decay of unmixed $B^0 \bar{B}^0$ or $B^+ B^-$ and the other is from a semileptonic $B$ decay. Though background $\Delta z$ distributions are estimated using MC simulations, the MC underestimates the width of the $\Delta z$ distribution. To correct for this, the MC $\Delta z$ distribution is convolved with a Gaussian of standard deviation $\sigma = 69$ $\mu$m [12]. The $\Delta z$ distribution for the true same-sign dilepton events, where positive ($++$) and negative ($--$) samples are combined, is shown in Fig. 8(a) together with the fit results. The $\chi^2/\text{n.d.f.}$ of the fit is 48.75/38 (note that only statistical errors are included). In the fit, the ratio of CT to WT is fixed at the
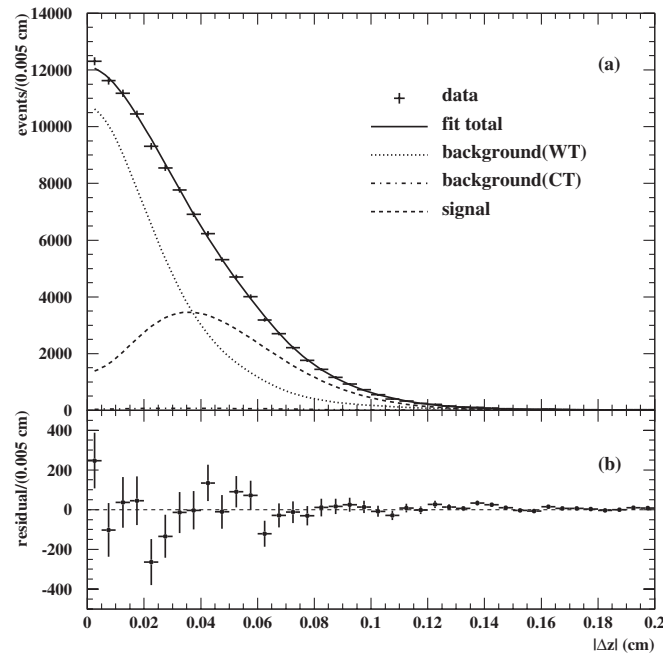
MC value, and only the ratio of signal and background is allowed to float. The MC-estimated CT and WT contributions to the $\Delta z$ distribution are shown in Fig. 8(a).

### C. Charge asymmetry

The $\Delta z$ dependence of the measured same-sign dilepton charge asymmetry ($A_{\ell\ell}(\Delta z)$) is defined as

$$A_{\ell\ell}(\Delta z) = \frac{N^{++}(\Delta z) - N^{--}(\Delta z)}{N^{++}(\Delta z) + N^{--}(\Delta z)}, \qquad (9)$$

where $N^{\pm\pm}(\Delta z)$ are the true dilepton yields as a function of $\Delta z$.

Since $N^{\pm\pm}(\Delta z)$ are the sum of signal and background, $N^{\pm\pm}(\Delta z) = N_s^{\pm\pm}(\Delta z) + N_b^{\pm\pm}(\Delta z)$, the $\Delta z$ bin-by-bin dilepton charge asymmetry $A_{\text{sl}}(\Delta z)$ is related to $A_{\ell\ell}(\Delta z)$ by

$$\begin{aligned} A_{\ell\ell}(\Delta z) &= \frac{N_s^{++}(\Delta z) - N_s^{--}(\Delta z)}{N_s(\Delta z)} \frac{N_s(\Delta z)}{(N_s(\Delta z) + N_b(\Delta z))} \\ &= A_{\text{sl}}(\Delta z) d(\Delta z) \end{aligned} \qquad (10)$$

where $N_s(\Delta z) = N_s^{++}(\Delta z) + N_s^{--}(\Delta z)$ and $N_b(\Delta z) = N_b^{++}(\Delta z) + N_b^{--}(\Delta z)$. Here, $N_b^{++}(\Delta z) = N_b^{--}(\Delta z)$ is assumed. A dilution factor, $d(\Delta z) = N_s(\Delta z)/(N_s(\Delta z) + N_b(\Delta z))$, is calculated using the signal and background yields, which are determined in the fit given in Fig. 8(a). The result for $A_{\text{sl}}(\Delta z)$, determined from the measured $A_{\ell\ell}(\Delta z)$ and $d(\Delta z)$, is shown in Fig. 9.

The dilepton charge asymmetry $A_{\text{sl}}$ is a time integrated quantity and does not depend on $\Delta z$. Averaging $A_{\text{sl}}(\Delta z)$ to a constant in the region 0.015 cm $< |\Delta z| <$ 0.200 cm yields $A_{\text{sl}} = (-1.1 \pm 7.9) \times 10^{-3}$, with a $\chi^2/\text{n.d.f.}$ of



FIG. 8. (a) $\Delta z$ distribution for the true dilepton events ($++$ and $--$ are combined). Points with error bars are data. The dot-dashed line shows the contribution from CT backgrounds, the dotted line shows the WT background contributions, the dashed line indicates the signal component and the solid line indicates the fitted total. (b) Difference between data and fit result as a function of $|\Delta z|$.
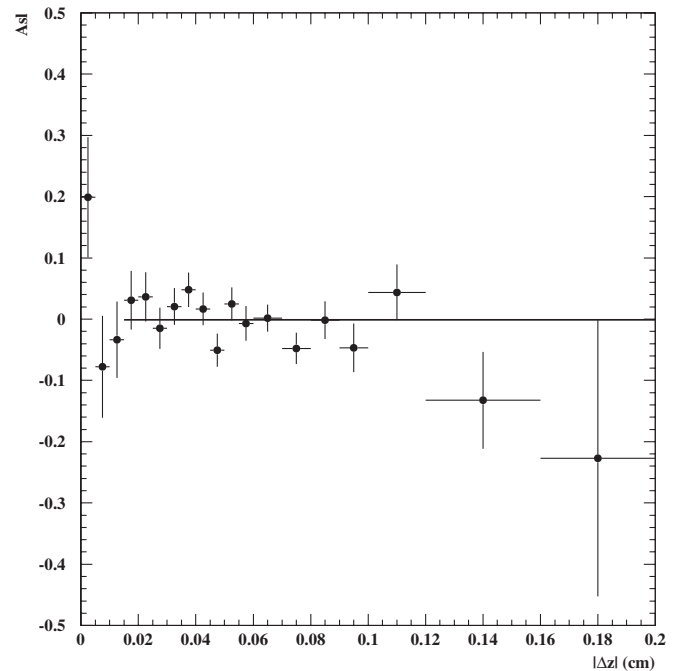


FIG. 9. $A_{\text{sl}}$ as a function of $|\Delta z|$.

36.20/36 (again note that only statistical errors are included). The $\Delta z$ range over which to determine $A_{sl}$ was chosen to minimize the combined statistical and systematic errors base on a MC study.

### D. Cross checks

As a consistency check, $A_{sl}$ is obtained separately for the $ee$, $\mu\mu$, and $e\mu$ data samples. The results, $A_{sl}^{ee} = (-13.3 \pm 14.4) \times 10^{-3}$, $A_{sl}^{\mu\mu} = (+16.5 \pm 17.3) \times 10^{-3}$, and $A_{sl}^{e\mu} = (-3.6 \pm 11.3) \times 10^{-3}$, are consistent with the primary result. Here the errors are statistical only.

The validity of the assumption of $N_b^{++}(\Delta z) = N_b^{--}(\Delta z)$, to extract $A_{sl}$ from $A_{\ell\ell}(\Delta z)$, is confirmed by repeating the fit without it. This yields $N_b^{++} = 20200 \pm 212$ and $N_b^{--} = 19766 \pm 210$ in the range $0.015 \text{ cm} < |\Delta z| < 0.200 \text{ cm}$, which is consistent with the initial assumption.

### E. Systematic errors

Systematic errors in the determination of $A_{sl}$ come from uncertainties in: (i) the event selection criteria; (ii) the continuum subtraction; (iii) efficiencies of track finding and lepton identification and hadron misidentification; (iv) the dilution factor determination; and (v) the $\Delta z$ range used for the determination of $A_{sl}$.

Uncertainties in the selection criteria are estimated by repeating the analysis with different threshold values. For the track selection, the $\theta_{lab}$ lower (higher) limit is varied from the nominal 30° (135°) to 40° (125°) in ten (eight-

een) steps, the closest-approach criterion in $r$-$\phi$ from its nominal value of 0.05 cm to 0.02 cm in 14 steps, the closest-approach criterion in $r$-$z$ from 2 cm to 1 cm in 14 steps, the $p^*$ lower (higher) limit from its nominal value of 1.2 GeV/$c$ (2.3 GeV/$c$) to 1.3 GeV/$c$ (2.2 GeV/$c$) in 14 steps, the requirement on the number of SVD hits by $\pm 1$ from its nominal value of greater than or equal to two for $r$-$z$ and one in $r$-$\phi$. For the event selection, the $\cos\theta_{\ell\ell}^*$ lower (higher) criterion is varied from nominal $-0.80$ ( $+0.95$) to $-0.60$ ( $+0.70$) in 12 (seventeen) steps. In addition, the mass windows that reject $J/\psi$ and $\gamma \to e^+e^-$ are widened by 20% and 50%, respectively.

To estimate the systematic error from the continuum subtraction, the analysis is repeated, varying the off-resonance yield by $\pm 1\sigma$.

Since the track finding efficiencies are determined using simulated tracks, we have examined the asymmetry of the track finding efficiencies using experimental data by comparing the yields of positive and negative tracks in the hadronic event sample. No requirement is imposed for the particle species. We expect no charge asymmetry of physics origin in particles from $B\bar{B}$ decays. We extract the charge asymmetry in the $B\bar{B}$ sample by subtracting the yield for off-resonance data from that for on-resonance data after correcting for the luminosity and cross section differences. The result shows presence of $0.25 \pm 0.09\%$ positive asymmetry. This can be attributed to asymmetry in the track finding efficiency or due to nuclear interactions which hadron tracks experience as they pass the detector materials. The size of the observed asymmetry is consistent

TABLE II. Source of systematic errors for the measurement of $A_{sl}$.

| Category | Source | $\Delta A_{sl}$ ( $\times 10^{-3}$) |
|---|---|---|
| Event selection | Track selection | $\pm 2.61$ |
| | $\cos\theta_{\ell\ell}^*$ cut | $\pm 0.63$ |
| | Lepton pair veto | $\pm 2.33$ |
| Continuum subtraction | | $\pm 4.88$ |
| Track corrections | Track finding efficiency | $\pm 5.06$ |
| | Electron identification efficiency | $\pm 0.56$ |
| | Muon identification efficiency | $\pm 1.98$ |
| | Fake electrons | $\pm 0.45$ |
| | Fake muons | $\pm 0.81$ |
| | Relative multiplicity | $\pm 0.56$ |
| | Model dependence | $\pm 0.75$ |
| $\Delta z$ fit for dileptons | Detector response function | $\pm 0.07$ |
| | $\Delta m_d$ | $\pm 0.08$ |
| | $\tau_{B^0}$ | $\pm 0.07$ |
| | 69 $\mu$m smearing of background $\Delta z$ | $\pm 0.13$ |
| | Statistics of signal MC | $\pm 0.01$ |
| | Statistics of background MC | $\pm 0.19$ |
| | Dilution factor fitting range | $\pm 0.04$ |
| | Assuming $N_b^{++} = N_b^{--}$ | $\pm 1.59$ |
| $A_{sl}$ average | $\Delta z$ range | $\pm 1.30$ |
| Total | | $\pm 8.51$ |

with the nuclear interaction effect. However, a precise estimation of nuclear interactions is rather difficult. Therefore, we conservatively include the effect of the above asymmetry to $A_{sl}$ as systematic error due to track finding efficiency.

For systematic uncertainties arising from the corrections to lepton candidates, we consider separately the effects due to the uncertainties in each bin and possible correlated sources of error. The errors of fake rates from pions, kaons and protons and the lepton identification efficiencies are assumed to be independent since they are dominated by statistical errors of control samples. The systematic uncertainties from these track corrections are estimated by varying the efficiencies and fake rates by $\pm 1\sigma$ bin-by-bin. The systematic effects associated with the relative hadron multiplicities are estimated by varying the values by $\pm 1\sigma$ for all bins (both electron and muon) simultaneously. The uncertainties for each hadron species are estimated separately, assuming that the multiplicities of each are uncorrelated. The systematic from model dependence in the MC is estimated by comparing the results from two different MC.

The contribution from the detector $\Delta z$ response function is estimated by changing the response function shape according to the statistics of each $\Delta z$ bin of $J/\psi \rightarrow \ell^+ \ell^-$ sample. The contribution from the 69 $\mu$m smearing is estimated by repeating the analysis with 43 $\mu$m and 96 $\mu$m smearing, corresponding to the uncertainty in the difference of the resolution between data and MC. The contributions from uncertainties in $\Delta m_d$ and $\tau_{B^0}$ are also estimated by varying the nominal values by $\pm 1\sigma$. The fitting range of the dilution factor determination is varied from its nominal range of 0.000 cm $< |\Delta z| <$ 0.200 cm to 0.025 cm $< |\Delta z| <$ 0.200 cm. The systematic uncertainty by assuming $N_b^{++} = N_b^{--}$ is estimated by calculation. For the choice of $\Delta z$ range used for the determination of $A_{sl}$, the lower limit is varied from 0.000 cm to 0.045 cm in nine steps. The results of the systematic error determination for $A_{sl}$ are summarized in Table II.

## V. CONCLUSION

The charge asymmetry for same-sign dilepton events from $\Upsilon(4S)$ decays has been measured. The result is related to the *CP* violation parameter in $B^0 - \bar{B}^0$ mixing,

$$A_{sl} = (-1.1 \pm 7.9(\text{stat}) \pm 8.5(\text{sys})) \times 10^{-3}, \quad (11)$$

corresponding to a 90% confidence level limit of $-2.01\% < A_{sl} < 1.80\%$ or equivalently

$$|q/p| = 1.0005 \pm 0.0040(\text{stat}) \pm 0.0043(\text{sys}). \quad (12)$$

The measured $A_{sl}$ is consistent with zero, or equivalently,

TABLE III. Comparison of the $\text{Re}(\epsilon_B)/(1 + |\epsilon_B|^2)$ measurements.

| Experiment | $\text{Re}(\epsilon_B)/(1 + |\epsilon_B|^2)$ |
|---|---|
| ALEPH | $-0.003 \pm 0.007$ |
| CLEO | $0.0035 \pm 0.0103 \pm 0.0015$ |
| *BABAR* | $(1.2 \pm 2.9 \pm 3.6) \times 10^{-3}$ |
| This experiment | $(-0.3 \pm 2.0 \pm 2.1) \times 10^{-3}$ |

$|q/p|$ is consistent with unity. This implies that *CP* violation in $B^0 - \bar{B}^0$ mixing is below the $O(10^{-2})$ level. The *CP* violation parameter $\epsilon_B$ can be calculated as

$$\frac{\text{Re}(\epsilon_B)}{1 + |\epsilon_B|^2} = (-0.3 \pm 2.0(\text{stat}) \pm 2.1(\text{sys})) \times 10^{-3},$$

$$(13)$$

using the (exact) formula

$$\frac{\text{Re}(\epsilon_B)}{1 + |\epsilon_B|^2} = 0.5 \frac{1 - \sqrt{(1 - A_{sl})/(1 + A_{sl})}}{1 + \sqrt{(1 - A_{sl})/(1 + A_{sl})}}. \quad (14)$$

These results are consistent with previous measurements [13] and provide significantly more restrictive bounds. Previous measurements of $\text{Re}(\epsilon_B)/(1 + |\epsilon_B|^2)$ are listed in Table III together with this measurement.

[1] A. B. Carter and A. I. Sanda, Phys. Rev. Lett. **45**, 952 (1980); Phys. Rev. D **23**, 1567 (1981).

[2] R. N. Cahn and M. P. Worah, Phys. Rev. D **60**, 076006 (1999); Y. Nir, hep-ph/9911321, and references therein.

[3] See, for example, A. Mohapatra, M. Satpathy, K. Abe, and Y. Sakai, Phys. Rev. D **58**, 036003 (1998), and references therein.

[4] M. Beneke, C. Buchalla, A. Lenz, and U. Nierste, Phys. Lett. B **576**, 173 (2003); M. Ciuchini, V. Lubicz, and C. Tarantino, J. High Energy Phys. 08 (2003) 031.

[5] S. Laplace, Z. Ligeti, Y. Nir, and G. Perez, Phys. Rev. D **65**, 094040 (2002), references therein.

[6] A. Abashian *et al.* (Belle Collaboration), Nucl. Instrum. Methods Phys. Res., Sect. A **479**, 117 (2002).

[7] S. Kurokawa and E. Kikutani, Nucl. Instrum. Methods Phys. Res., Sect. A **499**, 1 (2003), and other papers included in this volume.

[8] K. Hanagaki *et al.*, Nucl. Instrum. Methods Phys. Res., Sect. A **485**, 490 (2002).

[9] A. Abashian *et al.*, Nucl. Instrum. Methods Phys. Res., Sect. A **491**, 69 (2002).

[10] G. C. Fox and S. Wolfram, Phys. Rev. Lett. **41**, 1581 (1978).

[11] S. Eidelman *et al.* (Particle Data Group), Phys. Lett. B **592**, 1 (2004).

[12] N. C. Hastings *et al.* (Belle Collaboration), Phys. Rev. D **67**, 052004 (2003).

[13] F. Abe *et al.* (CDF Collaboration), Phys. Rev. D **55**, 2546 (1997); G. Abbiendi *et al.* (OPAL Collaboration), Eur. Phys. J. C **12**, 609 (2000); R. Barate *et al.* (ALEPH Collaboration), Eur. Phys. J. C **20**, 431 (2001); D. E. Jaffe *et al.* (CLEO Collaboration), Phys. Rev. Lett. **86**, 5000 (2001); B. Aubert *et al.* (*BABAR* Collaboration), Phys. Rev. Lett. **88**, 231801 (2002).